Ground-based cloud observation using wide-view optical and thermal representations

Dimitrios Tsourounis[1], Panagiotis Tzoumanikas[2], Alexios Kotronis[3], Orestis Panagopoulos[2], Andreas Kazantzidis[2], George Economou[1], and Christos Theocharatos[3*]

[1] Electronics Laboratory, Physics Dept., University of Patras, Rio Patras 26504, Greece,
[2] Laboratory of Atmospheric Physics, Physics Dept.,University of Patras,Rio Patras 26504 Greece,
[3] Irida Labs, Patras InnoHub – Kastritsiou 4, Magoula Patras 26504, Greece
dtsourounis@upatras.gr, tzumanik@ceid.upatras.gr, up1066667@upatras.gr, orestis.panagopou@upatras.gr, akaza@upatras.gr, economou@upatras.gr, htheohar@iridalabs.com

Abstract

A ground-based cloud observation system was developed in the context of the DeepSky project that utilizes optical and thermal cameras to capture wide-view images of the sky. A large dataset is created consisting of patch sky images in two modalities along with corresponding cloud category labels. Convolutional neural network models were trained using this dataset to classify the images into the cloud categories. Results highlight the complementary nature of the optical and thermal images in the task of cloud type classification.

1 Introduction

Clouds are collections of water droplets or ice crystals, and they form through the condensation of water vapor in the atmosphere, as it rises and cools, attaching to particles like dust, ice or sea salt and becoming visible [Liou1992]. Hence, there are various types of clouds according to multiple natural factors affecting their formation. The clouds significantly influence Earth's weather patterns, impacting the hydrological cycle, energy balance, and climate system. Consequently, accurate cloud observation is crucial for weather monitoring and relevant applications (e.g., air traffic control) as well as climate assessment or projections. Observation methods include space-based satellites, air-based radiosondes, and ground-based remote sensing. Satellite observations provide broad coverage, but they often lack the necessary temporal and spatial resolutions for localized and short-term cloud analysis. Air-based radiosonde observations excel in detecting cloud vertical structures however they

[*] Masterminded EasyChair and created the first stable version of this document

are costly. In response, ground-based remote sensing technologies offer cost-effective solutions with high-resolution images for detailed analysis of local cloud characteristics [Kazantzidis2012].

2 System

Our ground-based cloud observation system is equipped with two camera sensors, an optical camera and a Thermal-InfraRed (TIR) camera. The optical camera, also known as an Red Green Blue (RGB) camera, captures images using visible light (390 – 770 nm), similar to how our eyes perceive the world. It measures the intensity of red, green, and blue light to create a color image. On the other hand, the infrared camera, also referred to as a thermal camera, detects infrared radiation (8 – 14 μm) emitted by the atmosphere and clouds. It measures the heat emitted by different objects and converts it into an image displaying variations in temperature. The spectral band of 8–14 μm is known as the Long Wave InfraRed (LWIR), which is an ideal spectral range for cloud observation. In this spectral window, the atmosphere has low emission and high transmittance while clouds emit strong infrared radiation. Clouds could be considered as black-bodies since the optically thick clouds' emission is similar to a black-body at or near the temperature of the clouds [Shaw2012].

Both cameras have their advantages and limitations. The optical camera relies on visible light, which means it is influenced by factors like sunlight and atmospheric haze, affecting the pixel values. Furthermore, it operates effectively only during daylight hours. Nonetheless, the optical camera can capture texture patterns of clouds that are derived from sunlight and cloud thickness. On the other hand, the saturation problem of circumsolar region is avoided when images captured from thermal cameras. Moreover, thermal representations of clouds may lack detailed texture information, especially in cases where large areas of the clouds have similar temperatures. However, these images are affected less by the atmospheric aerosols while the most important advantage is the capture of images under various air conditions during day and night.

The use of a TIR microbolometer in thermal cameras necessitates a germanium lens, increasing the camera's cost significantly. This cost escalation is due to the necessity of custom-made lenses to achieve a wide Field of View (FoV) and high resolution [Klebe2014]. In the work of Wang et al. [Wang2021], a self-made dual system, comprising TIR and optical all-sky view cameras, is a noteworthy example. While this system provides all sky imagery and high resolution, the number of collected images is relatively small covering a few months recordings and thus, its cloud recognition approach relies on meteorological models that are regulated by local environmental conditions. Some other approaches have employed multiple cameras and scanning operation in different zenith directions [Sun2011] or utilized spherical aluminum mirrors to reflect the sky [Aebi2018] however, these methods introduce many challenging installation issues, such as the need for motoring mechanism, combining multiple captured images into a unified image, cleaning the mirror, and determining the appropriate distance between camera and mirror.

The DeepSky dual camera system we employed consists of an optical and a thermal sensor, both offering a wide-angle FoV and capturing registered images with a small scaling factor between them. This system is based on the Mobotix M73 cameras configuration. More specifically, the optical camera is equipped with an IR cut filter, enabling its use in small luminance conditions. The thermal sensor operates in the infrared range of 7.5 to 13.5 μm and exhibits a Noise-Equivalent Temperature Difference (NETD) sensitivity of 50 mK. This thermal camera is enhanced with integrated Thermal Radiometry technology and a high-end thermal image sensor that is calibrated to measure thermal radiation across the entire image area and assign a temperature value per pixel. A summary of the key specifications of this dual camera system is presented in the following Table 1. Furthermore, our novel recognition system, designed for image processing, is firmly rooted in the principles of deep learning, leveraging a vast number of annotated images from both modalities for robust performance.

Specs of Dual camera system	Optical Camera	Thermal Camera
Resolution (H × V in pixels)	640 × 480	640 × 480
Field of View (FoV) (H × V in degrees)	95º × 50º	90º × 69º
Focal Length	5mm	5mm
Aperture	f/1.8”	-
Operational Temperature	-40º to 60º C	
Protection	IP66, IK07	

Table 1: Key specifications of DeepSky dual camera system

3 Dataset

The DeepSky system captures Sky Patch Images (SPI) using wide-angle lenses for both the optical and thermal cameras. As a result, the images cover the central portion of the sky rather than entire sky, as our dual camera system is positioned to look directly overhead (zenith). This is in contrast to Total Sky Images (TSI), which use a hemispherical chrome-plated mirror to reflect the sky onto a downward-pointing camera located above the mirror, and All Sky Images (ASI) which are typically obtained using a camera equipped with a fish-eye lens [Nie2022]. The images captured by the DeepSky system, located at the Physics Department of the University of Patras (38° 17' 29" N, 21° 47' 20" E), and covers the period between 2022 and 2023. The images are labeled with one of the five cloud categories: cumulus, altocumulus, cirrus, clear sky, and stratocumulus-cumulonimbus, based on the classification recommended by the World Meteorological Organization (WMO). The classification of the images was performed by professional human observers from the Laboratory of Atmospheric Physics. Since both optical and thermal images are captured simultaneously, the cloud labels are associated with both image types. Therefore, images for daytime data of thermal camera are used because only daytime images are available for the visible camera and human annotation. To ensure balanced training data, an equal number of images was selected from 2022 for training. This was achieved by randomly choosing images according to the number of the smallest class, ensuring that each class had the same number of training samples. For the test set, all available images from 2023 were used. However, since the clear sky class was overrepresented, a subset of randomly selected clear sky images was reduced in order to maintain a more balanced distribution across all classes. Table 2 provides a description of each cloud category along with the number of images

Cloud types - Classes	Description	Training (during 2022)	Test (during 2023)
I) Cumulus	Low clouds, Fluffy and puffy clouds with a distinct dome-shaped appearance	278	82
II) Altocumulus	Middle clouds, Patched clouds with mosaic-like appearance	259	87
III) Cirrus	High clouds, Thin, wispy, and fibrous clouds with a feathery or filamentous appearance	275	70
IV) Clear sky	Cloudless sky or a very few cloudiness	286	426
V) Stratocumulus-Cumulonimbus	Low clouds, Thick and lumpy clouds with almost to mostly overcast	223	93
Total		1321	758

Table 2: Information about the DeepSky dual representation dataset

available for each category. It's important to note that the total number of images in the dataset is doubled due to the inclusion of both optical and thermal images. This dataset consists of SPI with two modalities, optical and thermal, and includes the corresponding cloud category labels. Figure 1 shows some examples of the images in the dataset.

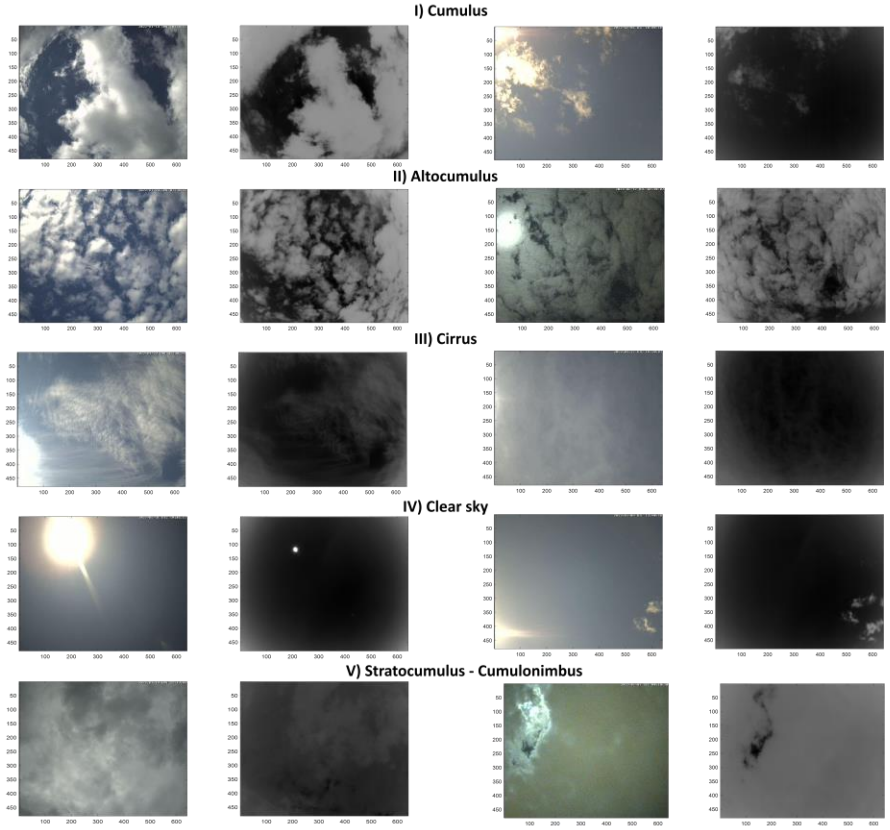

Figure 1: Examples of image pairs from the dual dataset with two modalities: optical (RGB images) and thermal (images with color scaling using a grayscale colormap). We display ten image pairs representing five cloud categories, with the RGB image on the left and the corresponding thermal image on the right.

4 Results

We employed a Convolutional Neural Network (CNN), specifically the ResNet-50 [He2016], to analyze the classification performance. Two separate CNN models were trained and evaluated using the optical and thermal images respectively. The images were resized to 224 x 224 pixels to reduce the computational cost. Also, the images are augmented by random horizontal and vertical flips during training. To ensure a coherent temperature range, the thermal images underwent pre-processing to limit temperature range between -80 and 25 degrees Celsius, where values exceeding 25 degrees were set to 25. This pre-processing step was necessary to eliminate temperature values that could be influenced by external factors such as a portion of sunlight or objects, like airplanes,

ensuring a more reliable and accurate analysis of the thermal data. The histograms of temperature values for the various cloud categories, generated using the training thermal images, provide a clear justification of this process, as shown in Figure 2. All images were normalized using mean subtraction and standard deviation division, calculated from the training data, before their input to CNN models.

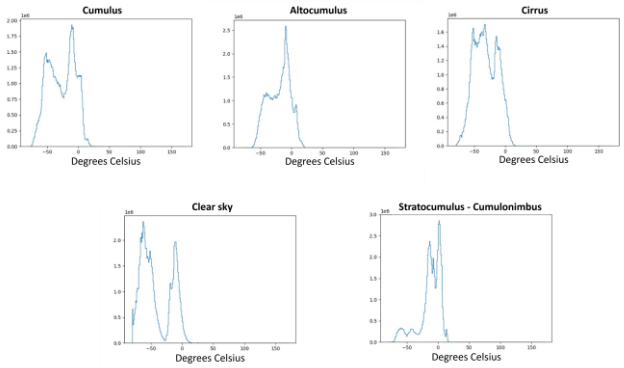

Figure 2: Histogram of temperature values in the thermal images for the five different cloud types presented in the training set of the dataset.

Optimization was performed by minimizing the cross-entropy classification loss with the RMSprop optimizer, employing a mini-batch size of 16 and an initial learning rate of 10^{-5} for 50 epochs. The classification results are presented using the confusion matrices in Figure 3 for the optical and thermal settings respectively. Although both CNN models achieved an average per-class classification accuracy of 76%, it is evident that optical and thermal representations have a different impact on the results. Specifically, the models performed similarly on cloudless sky (clear sky), middle clouds (altocumulus), and high clouds (cirrus). However, the classification accuracy for low clouds (cumulus and stratocumulus-cumulonimbus) differed between the two modalities. The model operating on optical images exhibited good performance in distinguishing cumulus clouds while the model operating on thermal images showed good performance in distinguishing stratocumulus-cumulonimbus clouds. This can be attributed to the information captured by each representation. The first model captured the texture and distinct features associated with cumulus clouds, such as clearly defined edges and white or light-gray color, whereas the second model detected the smaller temperature range (-30°C to 10°C) specific to stratocumulus-cumulonimbus clouds contrasting with the larger temperature range (-60°C to 10°C) observed in cumulus clouds.

5 Conclusions

In conclusion, a ground-based cloud observation system is developed incorporating optical and thermal cameras, enabling the capture of wide-view images of the sky. By utilizing this system, a substantial dataset comprising patch sky images in two modalities, along with associated cloud category labels, was created. Through the training of CNN models using this dataset, it was observed that the optical and thermal images complement each other in the classification of cloud types. This finding underscores the significance of utilizing multiple modalities for accurate and comprehensive cloud type classification. The integration of optical and thermal data enhances the overall understanding of cloud formations and contributes to advancements in cloud observation and analysis. Future plans include the fusion of both modalities into the training of a CNN as well as the extension of the dataset using a motor mechanism that moves the cameras into some predefined positions to capture complete view of the entire sky.

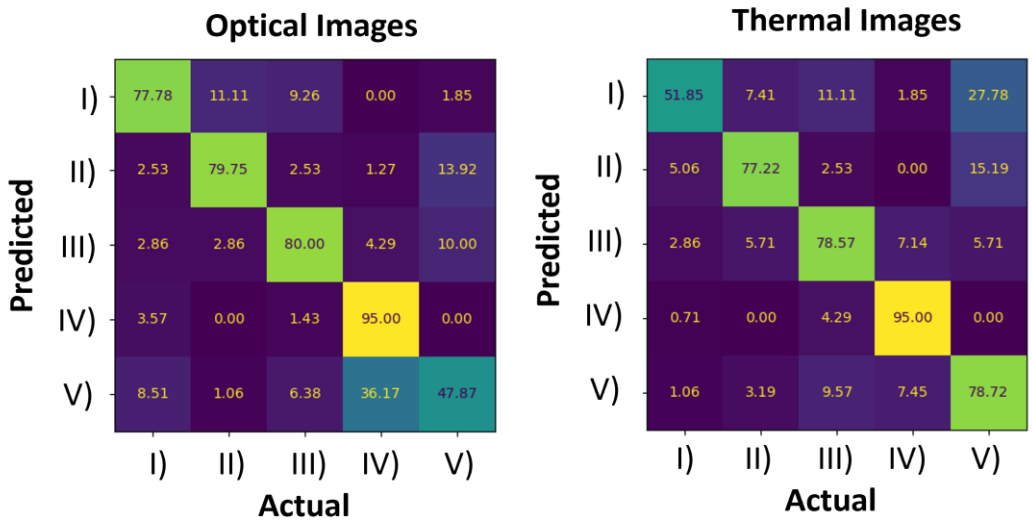

Figure 3: Confusion matrices using the Optical images (Left) and the Thermal images (Right).

Acknowledgments

This research has been co-financed by the European Union and Greek national funds through the Operational Program Competitiveness, Entrepreneurship and Innovation, under the call RESEARCH – CREATE – INNOVATE (project code: T1EDK – 00681, MIS 5067617).

References

Aebi, C., Gröbner, J., & Kämpfer, N. (2018). Cloud fraction determined by thermal infrared and visible all-sky cameras. *Atmospheric Measurement Techniques*, 11(10), 5549-5563.

He, K., Zhang, X., Ren, S., & Sun, J. (2016). Deep residual learning for image recognition. In *Proceedings of the IEEE conference on computer vision and pattern recognition* (pp. 770-778).

Kazantzidis, A., Tzoumanikas, P., Bais, A. F., Fotopoulos, S., & Economou, G. (2012). Cloud detection and classification with the use of whole-sky ground-based images. *Atmospheric Research*, 113, 80-88.

Klebe, D. I., Blatherwick, R. D., & Morris, V. R. (2014). Ground-based all-sky mid-infrared and visible imagery for purposes of characterizing cloud properties. *Atmospheric Measurement Techniques*, 7(2), 637-645.

Liou, K. N. (1992). Radiation and cloud processes in the atmosphere. Theory, observation, and modeling.

Nie, Y., Li, X., Paletta, Q., Aragon, M., Scott, A., & Brandt, A. (2022). Open-Source Ground-based Sky Image Datasets for Very Short-term Solar Forecasting, Cloud Analysis and Modeling: A Comprehensive Survey. arXiv preprint arXiv:2211.14709.

Shaw, J. A., & Nugent, P. W. (2013). Physics principles in radiometric infrared imaging of clouds in the atmosphere. *European Journal of Physics*, 34(6), S111.

Sun, X., Liu, L., & Zhao, S. (2011). Whole sky infrared remote sensing of cloud. *Procedia Earth and Planetary Science*, 2, 278-283.

Wang, Y., Liu, D., Xie, W., Yang, M., Gao, Z., Ling, X., ... & Xia, Y. (2021). Day and night clouds detection using a thermal-infrared all-sky-view camera. *Remote Sensing*, 13(9), 1852.